Hardware Setup of a Solar Microgrid Laboratory

Nicholas S. Coleman, Jesse Hill, Jonathan Berardino, Kara Lynne Ogawa, Ryan Mallgrave,
Ruben Sandoval, Yichen Qian, Lixin Zhu, Karen N. Miu and Chika Nwankpa
Department of Electrical and Computer Engineering, Drexel University
Philadelphia, PA, USA

***Abstract*—This paper outlines the hardware development of a solar microgrid laboratory at Drexel University. The renewable source for the microgrid is a 1.6 kW rooftop photovoltaic (PV) system. Various battery storage options and converter technologies can be connected to the PV source in order to supply the microgrid with DC or single-phase AC power. This paper details the laboratory environment, hardware testing, load profile development, and ongoing steps towards laboratory experiment development. The solar microgrid laboratory at Drexel University provides an environment for research and for undergraduate- and graduate-level experiential learning opportunities.**

I. Introduction

The Electric Power Research Institute (EPRI) estimates that $309-$403 billion in distribution research and infrastructure upgrades are required to realize the "smart grid" vision set forth by the U.S. Congress in 2007 [1], [2]. Microgrid projects, which support a greener and more reliable overall grid, are becoming increasingly prevalent ([3] lists over 70 operational microgrids in the U.S. alone) and will be significant contributions to the modernization of the overall grid.

Microgrids contain distributed resources and loads, and have the ability to operate in stand-alone or island mode [3]. Microgrids may also contain controllable loads in order to manage energy consumption under the uncertainty of distributed resources. In order to expose power engineering students to microgrid analysis and design tools, microgrid laboratory experiments are under development at Drexel University.

Other universities are also developing hardware and/or software microgrid laboratories. A software-based approach is outlined in [4]. Hardware-in-the-loop laboratories such as [5]–[7] enable testing with measurement and relaying equipment present in a practical full-scale microgrid. Integrated hardware laboratories with power electronic converters, renewable sources, and/or storage have been developed in [8]–[10].

Existing power systems laboratories at Drexel include the *I*nterconnected *P*ower *S*ystem *L*aboratory (IPSL) [11] and the *R*econfigurable *D*istribution *A*utomation and *C*ontrol (RDAC) Laboratory [12], [13]. Within IPSL, the Renewable Source Control Center (RSCC) [14] houses solar panels, batteries, and power electronic converters. RDAC is an interactive power distribution laboratory with reconfigurable networks and controllable loads.

A solar microgrid was made possible by installing an IPSL-RDAC interconnection. This paper outlines the hardware setup of the solar microgrid laboratory at Drexel University. A laboratory overview and hardware testing results are presented. An educational experiment, including a sample load profile designed around parameters obtained in hardware testing, is presented. The solar microgrid will provide students with the unique opportunity to work with real stochastic resources in a modular power system hardware environment.

II. Solar Microgrid Laboratory Overview

The solar microgrid integrates a 1.6 kW photovoltaic (PV) source, battery storage, and the necessary power electronic converters with the radial distribution network and user-selectable loads in RDAC. This section discusses the hardware environment of the microgrid laboratory.

RDAC is the backbone of the microgrid. Details of the original RDAC laboratory are available in [12], [13]. For reference, Fig. 1 provides the nominal three-phase AC configuration of a single RDAC station. Please note the bus labels; this nominal labeling scheme applies in any mode of operation. Individual nodes are labeled with their bus and phase (e.g., "node A2*b*" refers to the node on bus A2 that carries phase *b* under the nominal three-phase configuration). The remaining discussion will focus on DC and single-phase (1Φ) AC configurations.

A single-line diagram highlighting source and converter elements is provided in Fig. 2. Three "zones" exist in the solar microgrid. The solar panels are in zone 1 (rooftop). The battery and converters are housed in zone 2 (IPSL). Note that the battery and converter blocks are modular. Both lithium-ion and lead acid battery chemistries are available, and the inverter may be bypassed or swapped for one or more alternative converters to obtain the desired power type.

The IPSL-RDAC interconnection links zones 2 and 3. Zone 3 (RDAC) contains the distribution network and loads. Network switches and loads can be configured using automatic and/or manual control. The remainder of this section outlines the possible source, network, and load configurations.

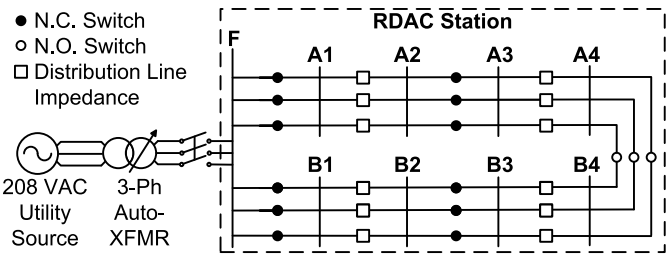

Fig. 1. Nominal three-phase configuration of an RDAC station with utility source [12] and one three-phase tie switch connecting buses A4 and B4. Up to four three-phase tie switches can be connected between any two buses.

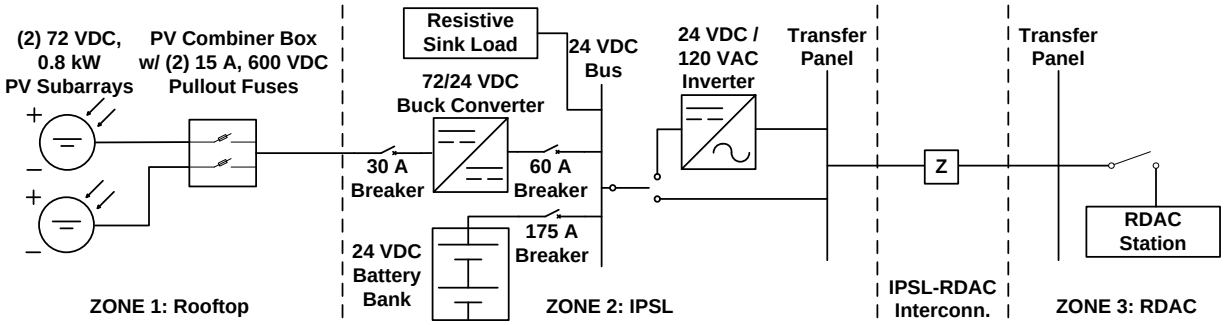

Fig. 2. Single-line diagram the solar microgrid illustrating the PV source, battery storage, and converters. Zone 1 (rooftop) includes two 0.8 kW PV sub-arrays and a fused combiner box. Zone 2 (IPSL) contains the storage and converter components. The IPSL-RDAC interconnection links zones 2 and 3, and has a non-negligible voltage drop, which is studied in this paper. Zone 3 (RDAC) contains the reconfigurable network and loads. The microgrid is almost completely reconfigurable; the pictured mode of operation uses an inverter to supply 1Φ 120 VAC to the RDAC network.

A. Source Configurations

In addition to the three-phase utility source (shown in Fig. 1), the following can presently be supplied to the microgrid:

- **120 VDC:** rectified utility output
- **72 VDC:** PV output
- **24 VDC:** battery and converted PV output
- **1Φ 120 VAC:** utility output
- **1Φ 120 VAC:** inverted PV+battery (as shown in Fig. 2)

B. Network Configurations

DC or 1Φ AC configurations are achieved by treating each three-phase RDAC bus as three separate nodes. Using all 27 physical nodes and two jumper cables, there are 648 DC or 1Φ configurations possible in each RDAC station. The jumper cables short together two pairs of physical nodes, leaving 25 electrical nodes to which the source can be connected, resulting in 16,200 possible source-and-network configurations. One radial 25-node example is shown in Fig. 3. Many more configurations are made possible by operating the sectionalizing and/or tie switches available in each station.

C. Loads

RDAC contains resistive (carbon filament light bulbs), inductive, and capacitive loads that can be connected to any node within a station. Loads may be arranged in single- or multi-phase configurations, and can be configured to create loads with specific characteristics. Manual switches and digital relays make both manual and automatic load control possible.

Additionally, specialized adapters allow devices with standard 2- or 3-prong North American electric plugs to connect to an RDAC station. These adapters can be used to interconnect small motor loads or power electronic devices, for example. Fig. 4 shows a cell phone being charged using the adapter. Digital relays can be used to switch plug-connected devices.

III. Hardware Testing

Testing of new and existing equipment was required. This section presents results for the following hardware deliverables:

- **Source characterization**: characterize the PV output under different seasonal conditions & become familiar with the vendor-provided battery management system (BMS) for a 24 VDC, 160 Ah lithium-ion battery.
- **Voltage drop testing**: perform AC and DC voltage drop testing over the IPSL-RDAC interconnection.

A. PV + Battery Source Characterization

First, we sought to gain an understanding of the power that could be expected from the rooftop PV array. Solar irradiation and power delivery measurements were collected during two seasons (winter and spring) with varying weather conditions.

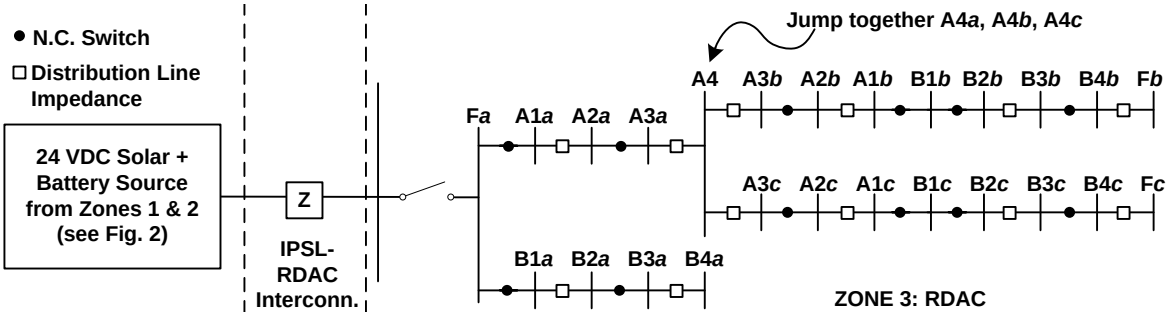

Fig. 3. Radial 25-bus DC or 1Φ AC configuration for a single RDAC station. This configuration can be obtained by: 1) connecting a 1Φ or DC source to phase *a* on bus F; and 2) by using jumper cables to connect the nodes A4*a*, A4*b*, A4*c*. The jumper cables are connected at binding posts (rated for 25 A), which are available at each bus; Fig. 4 includes a photograph of these binding posts.

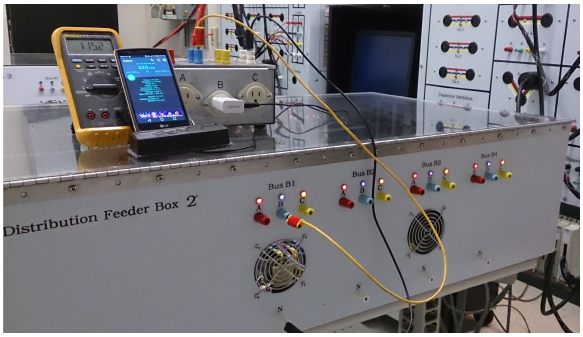

Fig. 4. A cell phone charging in RDAC through a plug adapter. The multimeter shows a node voltage of 115.2 VAC. A battery monitoring application on the cell phone shows a battery terminal voltage of 4.398 VDC and a charging current of 520 mA.

The hardware setup shown in Fig. 2 (including the 160 Ah lithium-ion battery bank) was used for this testing. An insolation meter measured solar irradiance at ground level in an unshaded parking lot approximately 150 meters from the solar panels. Voltage and current measurements at the 24 VDC bus in IPSL were used to find the power delivered to the microgrid network. A sink load was manually controlled to ensure that the battery bank state-of-charge (SOC) remained above the desired minimum.

Figs. 5 and 6 show winter and spring data, respectively. Data was collected for 3-4 hours starting shortly after 10:00 in order to observe the PV output around its typical daily peak. Source characterization data was used to select appropriate power and energy scales for three-hour load profiles, which are discussed further in Section IV

1) Observations:

- The mean observed solar injection was 1.03 kW on a cloudy February day, and 1.33 kW on a sunny May day, referred to the 24 VDC bus (i.e. after buck conversion).
- Considering a discharge efficiency of 97%, the fully-charged 160 Ah lithium-ion battery bank can supply approximately 2.79 kWh to the 24 VDC bus before reaching the minimum allowable SOC (25%).

2) Battery Management System (BMS): Another objective was to become familiar with the vendor-provided BMS. Fig. 7 shows a screen capture of the data that is available in real-time. Additional data is collected in log files. Relevant measurements include charging/discharging current, pack voltage (i.e. the total voltage across all the cells), and the SOC.

It was noted that SOC is not sensed, but estimated. The BMS initializes the SOC reading at 100%, regardless of the true SOC. The reading approaches a more reasonable value after some time, but this error makes it important to consider energy consumption in advance.

B. Voltage Drop Testing

Significant cabling was installed to create an interconnection that can deliver energy into RDAC from distributed sources. DC and 1Φ AC voltage drop tests were performed over each "phase" of this cabling in order to understand the power/energy losses that can be expected.

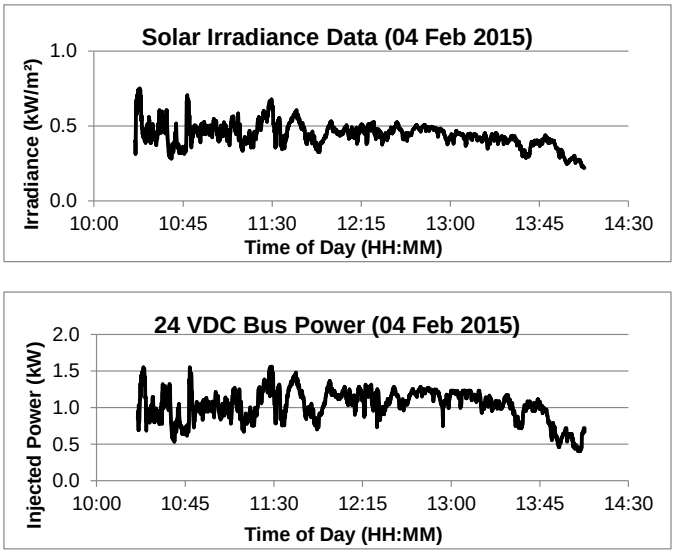

Fig. 5. Top: irradiance data. Bottom: real power data (one-minute simple moving average). Data obtained on 04 February 2015. Over 3.78 hours, the average power delivered to the 24 VDC bus was 1.03 kW.

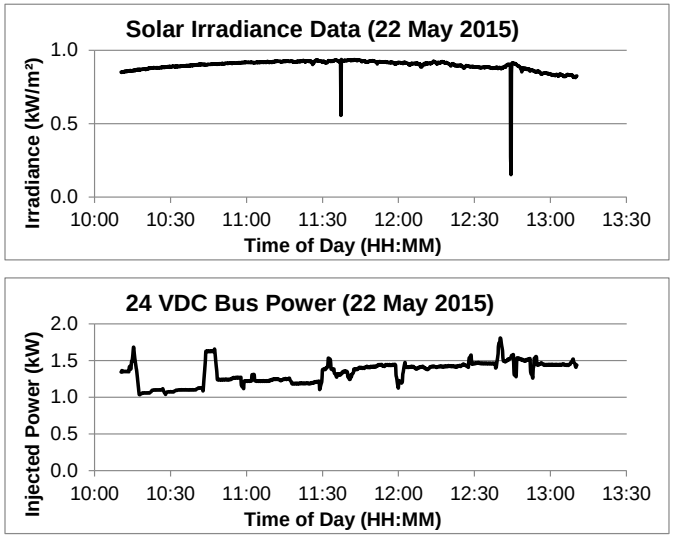

Fig. 6. Top: irradiance data. Bottom: real power data (one-minute simple moving average). Data obtained on 22 May 2015. Over 3.00 hours, the average power delivered to the 24 VDC bus was 1.33 kW.

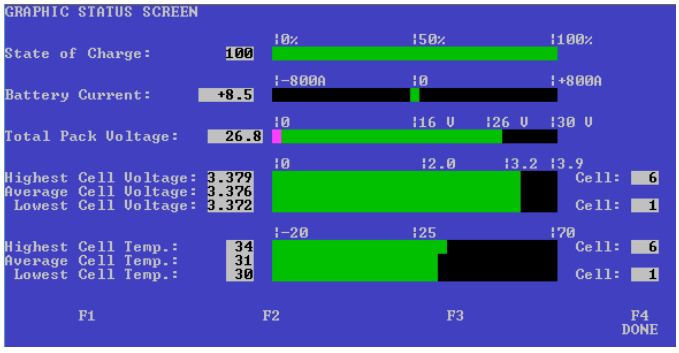

Fig. 7. Vendor-provided BMS screen for the 24 VDC, 160 Ah battery bank.

First, we tested the power handling capability of the interconnection. Each phase was tested by holding sending-end voltage at 120 V (RMS) and attaching a unity power factor load to the receiving end. The load was increased from 0 kW to 1.5 kW in 0.1 kW steps. Repeated sweeps confirmed that no voltage collapse occurred up to the 1.5 kW loading level; the maximum observed voltage drop was 2.0 V.

Next, constant load, variable voltage tests were performed to obtain impedance data. Each test was performed by attaching a fixed 1 kW load to the receiving end of the interconnection and sweeping the sending end voltage from 120 V to 70 V and back, in steps of 10 V (RMS). Five AC and DC sweeps were performed on each phase of the interconnection.

Sample data from phase *b* cabling (i.e. the cable which would normally carry phase *b* current under three-phase operation) is shown in Fig. 8.

Resistance R equals the slope of the least-squares best fit line through the origin and the ΔV vs. I data obtained during the DC test. Impedance magnitude $|Z|$ (at 60 Hz) equals the analogous slope obtained from the AC test. Then, 60 Hz reactance is calculated with:

$$X = \sqrt{|Z|^2 - R^2} \tag{1}$$

Results for all three cables are summarized in Table I.

C. Loss Characterization

In order to understand the PV+battery output required to meet demand in RDAC, conversion and delivery losses must be quantified as well. Demand in RDAC is limited by the maximum output of the source (Section III-A), and the following losses:

- **Conversion losses**: assumed equal power and energy efficiency of 81% for the 24 VDC/120 VAC inverter.
- **IPSL-RDAC interconnection losses**: estimated using cable resistances (Section III-B).
- **Network losses**: estimated using RDAC impedances [13].

Actual losses depend on weather and demand and must be estimated in terms of the load or expected load. This is discussed further in Sec. IV.

IV. Educational Experiment Development

Solar microgrid experiments will be designed to expose students to practical AC/DC microgrid analysis concepts, which are not necessarily covered in traditional transmission and distribution courses, including:

- Stochastic power sources
- Power electronic conversion basics
- Storage/load management

This section discusses one such experiment that addresses these educational concepts. In this experiment, students will model a residential load profile in RDAC and make real-time, weather-dependent control decisions. The experiment is intended for students who are familiar with the load control capabilities in RDAC [13].

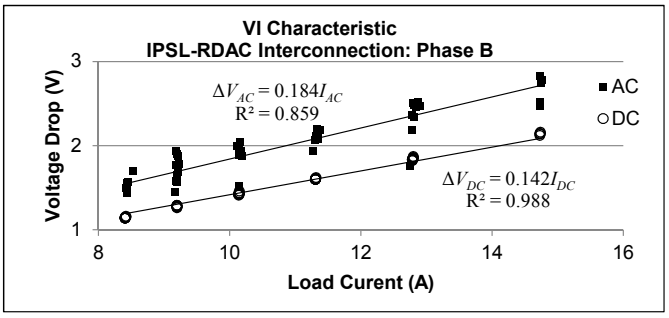

Fig. 8. 60 Hz AC and DC voltage drop data on phase *b* of the IPSL-RDAC interconnection. Load: constant 1.0 kW, 1.0 PF. Five voltage sweeps from 120 V to 70 V to 120 V (RMS) were conducted in 10 V steps.

TABLE I
IPSL-RDAC interconnection impedances at 60 Hz, observed over a current range of approximately 8-15 A RMS.

Phase	$\|Z\|$ (Ω)	R (Ω)	X (Ω)
a	0.167	0.141	0.089
b	0.184	0.142	0.117
c	0.187	0.138	0.126

A. Setup and Weather Conditions

The microgrid is configured as shown in Fig. 2 to supply 1Φ 120 VAC to zone 3 (RDAC). The 160 Ah battery bank is initially connected and fully charged. Considering the hardware testing results and time constraints, an appropriately scaled 24-hour load profile has been designed to yield these interesting weather-dependent scenarios:

- **"Nighttime" conditions** (i.e. zero PV power): curtailment is necessary. The SOC constraint will be activated if demand + losses exceeds 2.79 kWh.
- **Cloudy February conditions**: the load will be served, but with significant draw from the battery.
- **Sunny May conditions**: some transient battery discharge may be required, but the battery should have a near-full SOC by the end of the profile.

B. Prelab Assignment

Prior to the experiment, students will be introduced to basic source and converter theory. Students will use this theory and a provided 24-hour load profile to complete the following prelab tasks: 1) model the load profile using loads available in RDAC; 2) time-scale the load profile to fit within the 2-3 hour lab period; and 3) power-scale the load profile to a total energy consumption (including converter and I^2R losses) of approximately 3 kWh.

One scaled nominal profile, including load-dependent loss estimates, is presented in Fig. 9. Depending on weather conditions, one of the scenarios listed in Sec. IV-A will occur. Plot annotations highlight that: 1) maximum demand falls between the average winter and spring PV outputs observed in Section III-A; and 2) with zero PV supply and no curtailment, the battery will drain beyond the 25% SOC limit. Load profile parameters are summarized in Table II. Additional load

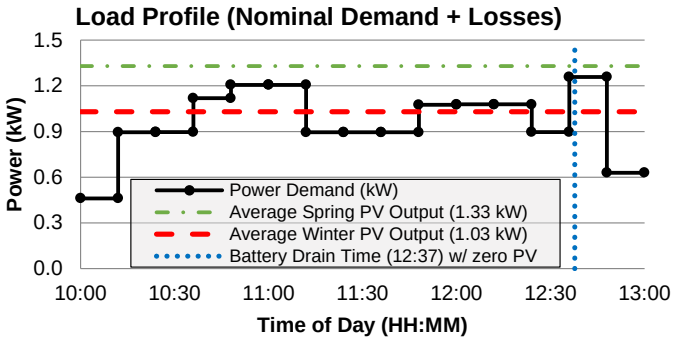

Fig. 9. Scaled nominal load profile. The dotted line indicates time of power lossdue to the SOC limit under "nighttime" conditions with no curtailment.

TABLE II
LOAD PROFILE PARAMETERS.

Parameter	Value (nominal)	Value + Losses†
Maximum Power	1.00 kW	1.27 kW
Average Power	0.77 kW	0.94 kW
Energy Use	2.45 kWh	3.02 kWh

†Estimated on phase *a*. See Sec. III-C for loss characterization.

profiles, including detailed breakdowns of the loads connected at any given time, are available in [15].

C. Laboratory Procedure and Learning Outcomes

Students manually adjust loads to follow their scaled load profiles. Load types and corresponding wattages are realized through watt-equivalent RDAC loads (e.g., to model appliances) and through the plug-adapter (see Fig. 4). In [15], the plug-adapter was used to interconnect a hair dryer (motor load) and a laptop (power electronic load), for example.

Throughout the experiment, students monitor real-time voltages and currents using the BMS and the RDAC distribution management system (DMS) [13]. Students use this data to confirm conversion/loss calculations, and to observe the impact of varying (stochastic) weather conditions. The battery SOC constraint ($\geq$25%), requires students to make real-time storage/load management decisions (e.g., curtailment or load shaping).

V. CONCLUSION

The hardware setup of a solar microgrid at Drexel University has been presented. The microgrid laboratory is flexible by design. Both DC and AC sources are possible, the network can be reconfigured, and a variety of loads can be connected and controlled either automatically or manually.

Major steps towards developing a working laboratory included characterizing source outputs, voltage drop testing, and loss characterization. A weather-dependent educational experiment has been presented. The solar microgrid laboratory will enable students and researchers to:

- analyze and operate a microgrid with a re-located source.
- evaluate the capability of an islanded system.
- study (bi-directional) injection prioritization/curtailment.
- research DC microgrid analysis and operation.
- characterize the "transmission line parameters" of the interconnect under different source types.

Ongoing work includes the development of 1) software-based simulations of the solar microgrid and 2) formal educational laboratory manuals. Completion of these steps will provide students with comprehensive hardware/software microgrid laboratory experiences to supplement traditional power systems engineering education.

ACKNOWLEDGMENT

The authors acknowledge the support of the National Science Foundation (grant no. DUE 1226126).

REFERENCES

[1] C. Gellings, "Estimating the Costs and Benefits of the Smart Grid," EPRI, Palo Alto, CA, Rep. 1022519, 2011.

[2] *An Act to move the United States toward greater energy independence and security, to increase the production of clean renewable fuels, to protect consumers, to increase the efficiency of products, buildings, and vehicles, to promote research on and deploy greenhouse gas capture and storage options, and to improve the energy performance of the Federal Government, and for other purposes*, Public Law 110-140, *U.S. Statutes at Large* 121 (2007): 1492-1801.

[3] A. Maitra, L. Rogers, R. Handa, "Program on Technology Innovation: Microgrid Implementations: Literature Review," EPRI, Palo Alto, CA, Rep. 3002007384, 2016.

[4] A. S. Deese, V. Cecchi, and B. Poudel, "Introduction of Emerging Technologies to Distribution System Laboratory Modules via Simulation," in *Proc. 2015 IEEE Power and Energy Soc. General Meeting*, Denver, CO, USA, 2015.
A. Pahwa, W.B. Kuhn, R.D. Miller, A. Rys, "Educational and research challenges and opportunities related to renewable energy," in *Proc. 2011 IEEE PES General Meeting*, Detroit, MI, USA, 2011.

[5] E.C. Piesciorovsky, N.N. Schulz, "Burns & McDonnell — K-State Smart Grid Laboratory: Protection, communication & power metering," in *Proc. 2014 IEEE PES General Meeting Conference & Exposition*, National Harbor, MD, USA, 2014.

[6] S. S. Biswas, J. H. Kim, and A. K. Srivastava, "Development of a Smart Grid Test Bed and Applications in PMU and PDC Testing," in *Proc. North Amer. Power Symp. (NAPS)*, Champaign, IL, USA, 2012.

[7] N. Yousefpoor, "Real-Time Hardware-in-the-Loop Simulation of Convertible Static Transmission Controller for Transmission Grid Management," in *IEEE 14th Workshop on Control and Modeling for Power Electron.*, Salt Lake City, UT, USA, 2013.

[8] A. S. Deese, "Development of Smart Electric Power System (SEPS) Laboratory for Advanced Research and Undergraduate Education," *IEEE Trans. Power Syst.*, vol.30, no.3, pp.1279-1287, May 2015.

[9] V. Salehi *et al.*, "Laboratory-Based Smart Power System, Part I: Design and System Development," *IEEE Trans. Smart Grid*, vol. 3, no. 2, pp. 1394-1404, Sep. 2012.

[10] M. Rasheduzzaman, B. H. Chowdhury, and S. Bhaskara, "Converting an Old Machines Lab Into a Functioning Power Network With a Microgrid for Education," *IEEE Trans. Power Syst.*, vol.29, no.4, pp. 1952-1962, July 2014.

[11] S. P. Carullo *et al.*, "Interconnected Power System Laboratory: Fault Analysis Experiment, *IEEE Trans. Power Syst.*, vol. 11, no. 4, Nov. 1996, pp. 1913-1917.

[12] X. Yang *et al.*, "Setup of RDAC — a Reconfigurable Distribution Automation and Control Laboratory", in *Proc. 2001 IEEE Power and Energy Soc. Summer Meeting*, Vancouver, BC, Canada, 2001. pp. 1524-1529.

[13] X. Yang *et al*, "Reconfigurable Distribution Automation and Control Laboratory: Multi-phase, Radial Power Flow Experiment," *IEEE Trans. Power Syst.*, vol. 20, no. 3, Aug. 2005, pp. 1207-1214.

[14] J. Hill, C. Nwankpa, "Hardware Platform for Testing Battery Energy Storage Systems in the Presence of Renewables," in *Proc. 2013 IEEE PowerTech Conference*, Grenoble, France, 2013.

[15] R. Mallgrave, Y. Qian, R. Sandoval, and L. Zhu, "Solar Power Distribution System," Senior Des. Rep., Dept. of Elect. and Comput. Eng., Drexel Univ., Philadelphia, PA, 2015.